Optics Communications 284 (2011) 3723–3736

Contents lists available at ScienceDirect

Optics Communications

journal homepage: www.elsevier.com/locate/optcom

Invited paper

Photonic generation of microwave arbitrary waveforms

Jianping Yao

Microwave Photonics Research Laboratory, School of Information Technology and Engineering, University of Ottawa, Ottawa, ON, Canada, K1N 6N5

ARTICLE INFO

Article history:
Received 15 December 2010
Received in revised form 23 February 2011
Accepted 24 February 2011
Available online 12 March 2011

Keywords:
Arbitrary waveform generation
Direct space-to-time pulse shaping
Fiber optics
Fiber Bragg grating
Microwave Photonics
Photonic microwave delay-line filter
Spectral-shaping and
wavelength-to-time mapping
Temporal pulse shaping

ABSTRACT

In this paper, techniques to generate microwave arbitrary waveforms based on all-fiber solutions are reviewed, with an emphasis on the system architectures based on direct space-to-time pulse shaping, spectral-shaping and wavelength-to-time mapping, temporal pulse shaping, and photonic microwave delay-line filtering. The generation of phase-coded and frequency-chirped microwave waveforms is discussed. The challenges in the implementation of the systems for practical applications are also discussed.

1. Introduction

Microwave arbitrary waveforms are widely used in radar, communications, medical imaging, and modern instrumentation systems. Microwave arbitrary waveforms are usually generated in the electrical domain using digital electronics. Due to the limited sampling rate, the generation of a microwave arbitrary waveform in the electrical domain is limited to a low frequency and small bandwidth. For many applications, however, high frequency and large bandwidth waveforms are needed. A solution is to generate microwave arbitrary waveforms in the optical domain, to take advantage of the high speed and broad bandwidth offered by modern optics. In general, photonically assisted microwave waveform generation can be classified into four categories, 1) direct space-to-time pulse shaping, 2) spectral-shaping and wavelength-to-time mapping, 3) temporal pulse shaping, and 4)microwave pulse generation based on photonic microwave delay-line filtering. These techniques can be implemented in free space where a spatial light modulator (SLM) is usually employed to perform temporal or spectral shaping. The key advantage of using an SLM in a microwave arbitrary waveform generation system is its flexibility. An SLM can be updated in real time, making the system reconfigurable. However, a pulse shaping system based on an SLM is usually implemented in free space, making the system bulky and costly. In addition, the coupling between fiber and free space and free space to fiber makes the system lossy and sensitive to environmental changes. Microwave arbitrary waveform generation can also be implemented using pure fiber-optic devices. Considering the low loss and small size, a microwave waveform generation system using fiber optic devices is considered a promising alternative to that implemented based on free space optics. In this paper, techniques to use fiber optic devices to implement arbitrary microwave waveform generation are reviewed. All the four different techniques that are implemented using fiber optic devices are discussed. The use of the techniques to generate frequency-chirped and phase-coded microwave waveforms is discussed. The challenges in implementation the systems for practical applications are also discussed.

2. Direct space-to-time pulse shaping

Arbitrary waveform generation can be realized based on direct space-to-time (DST) mapping [1–11], in which an arbitrary optical pulse sequence is generated in the optical domain and then applied to a high-speed optical-to-electrical converter to generate a microwave waveform. By this technique, reprogrammable cycle-by-cycle synthesis of an arbitrarily shaped phase-coded or frequency-chirped waveform could be implemented. In the system, a bandwidth-limited optical-to-electrical converter was usually used to convert an optical pulse burst consisting of isolated optical pulses into a smooth microwave waveform. Fig. 1 shows a DST mapping system in which an ultrashort optical pulse from a pulsed laser source is sent to an optical pulse shaper to generate a pulse burst, with the pulse spacing increasing temporally. The pulse burst is then applied to an optical-to-

E-mail address: jpyao@site.uottawa.ca.

0030-4018/$ – see front matter © 2011 Elsevier B.V. All rights reserved.
doi:10.1016/j.optcom.2011.02.069

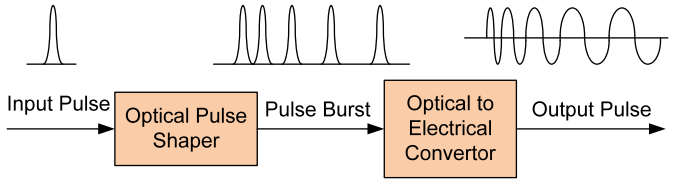

Fig. 1. Arbitrary waveform generation based on direct space-to-time (DST) mapping.

electrical converter or a photodetector (PD). Due to the bandwidth-limited nature of the PD, the high-frequency components are eliminated and a smooth frequency-chirped microwave waveform is generated.

The key device in the DST mapping system is the optical pulse shaper. It could be implemented using free-space optical components [1–8], but with large size, high loss and poor stability. A simpler but more effective solution is to generate a pulse burst using an arrayed waveguide grating (AWG) [9–11], as shown in Fig. 2. An ultra-short pulse is launched into the AWG through an amplitude mask. Due to the different time delays resulted from the different physical lengths of the waveguides in the AWG, a pulse burst with temporally spaced pulses is generated. To generate a pulse burst with the desired temporal pattern, the input amplitude mask can be configured to block the light from going into some of the optical waveguides. The use of the AWG-based pulse shaper to generate a pulse burst of more than 30 pulses as an ultrafast optical data packet over approximately an 80-ps temporal window was demonstrated [9]. The generation of high-repetition-rate femto-second WDM pulses was also demonstrated [10].

The theory behind the generation of a microwave arbitrary waveform using a DST mapping system is that the waveform to be generated can be obtained by filtering the pulse burst using a band-limited filter [12]. We recently demonstrated that a temporally spaced pulse burst, such as a pulse burst with increasing or decreasing temporal spacing, would have a multi-channel spectral response, with one channel having a spectrum that corresponds to the spectrum of the waveform to be generated [12]. Fig. 3 shows the generation of a linearly chirped microwave waveform from a pulse burst with increasing pulse spacing through bandpass filtering. As can be seen the +1st order channel has a spectral response that is equal to that of a linearly chirped microwave waveform. By employing a bandpass filter to select the +1st order channel, a linearly chirped microwave waveform would be generated. In the following, a brief mathematical derivation is provided to show the generation of an arbitrary microwave waveform through pulse position modulation [13] and bandpass filtering.

A uniformly-spaced intensity-modulated optical pulse burst $p_T(t)$, in which the kth pulse has a time delay of $\tau_k = kT$, where T is the time-delay difference between two adjacent pulses, can be expressed as

$$p_T(t) = \sum_{k=1}^{N} \alpha_k g(t-kT), \tag{1}$$

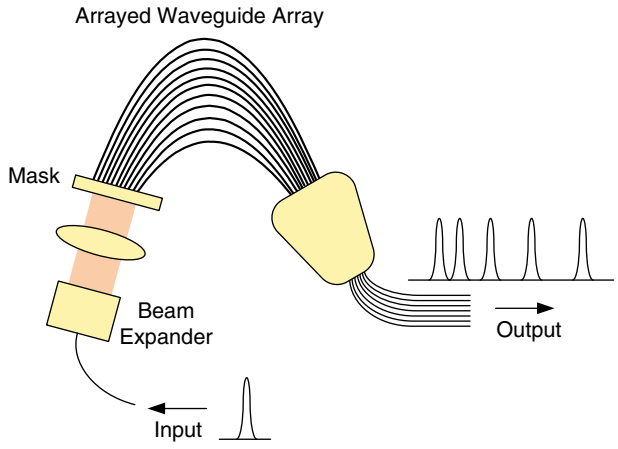

Fig. 2. Optical pulse shaper based on an arrayed waveguide array.

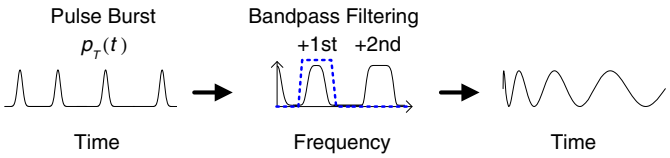

Fig. 3. Generation of a chirped microwave waveform from a pulse burst with increasing pulse spacing through bandpass filtering.

where $g(t)$ is a single short pulse, α_k is the coefficient weighted on the kth pulse, and N is the number of the pulses in the pulse burst. The pulse burst can be expressed in another form,

$$p_T(t) = g(t) * \sum_{k=1}^{N} \alpha_k \delta(t-kT) = g(t) * [a(t) \times s(t)] \tag{2}$$

where $a(t)$ is the weight profile which is given as $a(kT) = \alpha_k$ for $1 \le k \le N$, otherwise $a(t) = 0$; $s(t)$ is an unit impulse train given by $s(t) = \sum_k \delta(t-kT)$, and * denotes the convolution operation.

The spectrum of the pulse burst, $P_T(\omega)$, can be calculated by the Fourier transform,

$$P_T(\omega) = G(\omega) \times \left[\frac{1}{2\pi} A(\omega) * \sum_m \frac{2\pi}{T} \delta(\omega - m\Omega)\right] = \sum_m \frac{1}{T} G(\omega) A(\omega - m\Omega) \tag{3}$$

where $\Omega = 2\pi/T$, $A(\omega)$ is the Fourier transform of $a(t)$, and $G(\omega)$ is the spectrum of the short pulse $g(t)$. Since the pulse $g(t)$ is usually ultra-short, its spectrum $G(\omega)$ changes much slower compared with $A(\omega - m\Omega)$ within the bandwidth at Ω. Therefore, the change of $G(\omega)$ within the mth channel could be ignored, and $G(\omega)$ can be approximated as $G(m\Omega)$. Thus, the pulse burst has a multi-channel spectral response, with all channels having the same spectral profile $A(\omega)$ and the mth channel being located at $m\Omega$.

If a microwave bandpass filter with its bandpass located at $\omega = m\Omega$ is used in the system, the spectrum of the mth channel of the pulse burst is selected. As a result, the signal at the output of the microwave bandpass filter is given by

$$P(\omega) \approx \frac{1}{T} G(m\Omega) A(\omega - m\Omega). \tag{4}$$

In the time domain, the output microwave signal, $p(t)$, is the inverse Fourier transform of Eq. (4), which is given by

$$\begin{aligned} p(t) &= \frac{1}{T} G(m\Omega) a(t) \times \exp(jm\Omega t) \\ &= \frac{1}{T} G(m\Omega) |a(t)| \times \exp\{j[\varphi(t) + m\Omega t]\} \end{aligned} \tag{5}$$

where $\varphi(t)$ is the phase response of $a(t)$. We can clearly see that the output signal is a microwave signal with a central frequency located at $m\Omega$. The generated phase modulation is just the phase of the weight profile, $\varphi(t)$.

Based on Eq. (5), we can see if an arbitrary microwave waveform is generated then $a(t)$ should be a function having an arbitrary phase response. While in a DST mapping system, since only the power of the individual pulse is detected at the PD, the coefficients, α_k, are always positive. Therefore, the required phase response $\varphi(t)$ cannot be introduced. A solution to this problem is to introduce a phase shift through varying the spacing of the pulse burst, which is also called pulse position modulation. For a specific frequency, a time shift corresponds to

a phase shift, and the inclusion of the phase shift would make the weight profile be complex-valued, leading to the generation of an arbitrary microwave waveform.

Assume a function $f(t)$ is introduced to describe the pulse position modulation, that is, $s(t+f(t)) = \sum_k \delta(t+f(t)-kT)$, a new optical pulse burst is given by

$$\tilde{p}_T(t) = g(t) * \{a(t) \times s[t+f(t)]\}. \tag{6}$$

With the introduction of $f(t)$, the time spacing of the pulse burst is no longer uniform. Based on Fourier Series expansion, $s(t)$ can be expressed by its Fourier series, $s(t) = \sum_m \frac{1}{T}\exp(jm\Omega t)$. By variable substitution, Eq. (6) can be written as

$$\tilde{p}_T(t) = g(t) * \sum_m \frac{1}{T} a(t)\exp[jm\Omega f(t)] \times \exp(jm\Omega t). \tag{7}$$

Note that the above equation is obtained by variable substitution, it is no longer a Fourier series expansion (an aperiodic signal does not have a Fourier series expansion).

Since $g(t)$ is ultra-short, we may model it as an unit impulse, that is, $g(t)=\delta(t)$, where $\delta(t)$ is the Dirac delta function. Thus, Eq. (7) can be approximated as

$$\tilde{p}_T(t) \approx \sum_m \frac{1}{T} a(t)\exp[jm\Omega f(t)] \times \exp(jm\Omega t). \tag{8}$$

It is clearly seen from Eq. (8) that the nonuniformly-spaced pulse burst is expressed as the sum of multiple bandpass microwave signals with different central frequencies. If T is sufficiently small such that the mth channel is not interfered by its adjacent channels, the spectral component at $m\Omega$ can be filtered out by a microwave bandpass filter with its central frequency at $m\Omega$. Then the output microwave signal is now given by

$$\tilde{p}(t) = \frac{1}{T}\{a(t)\exp[jm\Omega f(t)]\} \times \exp(jm\Omega t). \tag{9}$$

Comparing Eq. (9) with Eq. (5), we can see that an additional phase modulation is introduced to the microwave signal due to the pulse position modulation introduced by $f(t)$. Therefore, although the weight coefficients are all positive, by using a specially designed pulse burst with pulse position modulation, an arbitrary microwave waveform can be obtained.

For example, to generate a phase-coded microwave waveform, if the phase modulation function is $\varphi(t)$, then the relationship between the pulse position modulation function $f(t)$ and the desired phase modulation can be obtained by letting $\varphi(t)=m\Omega f(t)$ or

$$f(t) = \frac{\varphi(t)}{m\Omega}. \tag{10}$$

Substituting Eq. (10) into Eq. (6), we get the time delay of each pulse in the pulse burst,

$$\tau_k + \frac{\varphi(\tau_k)}{m\Omega} = kT. \tag{11}$$

Considering the property of the Dirac function, the coefficients can also be obtained, which are given by

$$\alpha_k = \left|\frac{a(\tau_k)}{1+\varphi'(\tau_k)/m\Omega}\right|. \tag{12}$$

Based on the analysis we conclude that if a pulse burst with a pulse position modulation described by Eq. (11) with the coefficients given by Eq. (12), a microwave signal with a central frequency located at $m\Omega$ and a phase modulation of $a(t)\exp[j\varphi(t)]$ are then obtained at the output of a microwave bandpass filter with its central frequency located at $m\Omega$.

3. Spectral-shaping and wavelength-to-time mapping

Arbitrary waveform generation can be realized based on spectral-shaping and wavelength-to-time mapping. The fundamental principle of the technique is shown in Fig. 4(a). The system consists of a pulsed source, a spectral shaper and a dispersive element. The spectral shaper is used to modify the spectrum emitted from the pulsed laser source, which can be a passively or actively mode-locked laser source. The shaped spectrum then undergoes wavelength-to-time mapping in a dispersive device, which can be a length of dispersive fiber or a chirped fiber Bragg grating. A microwave waveform is generated in the electrical domain at a high-speed photodetector. If the dispersive element is a length of fiber with a value of dispersion of $\ddot{\Phi}$, for an input

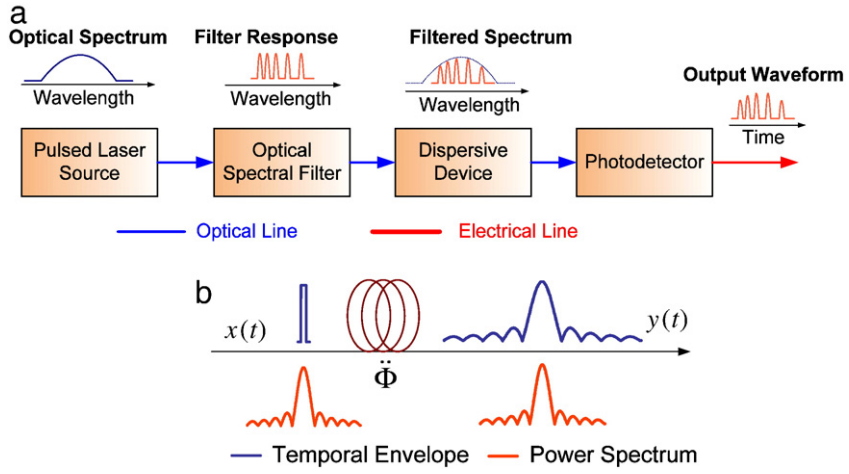

Fig. 4. Arbitrary waveform generation based on spectral-shaping and wavelength-to-time mapping. (a) Schematic of a microwave waveform generation system based on spectral-shaping and wavelength-to-time mapping. (b) Illustration of wavelength-to-time mapping in a dispersive element.

pulse $g(t)$ with a temporal width of Δt_0, the signal at the output of the dispersive element is given

$$y(t) = g(t) * \exp\left(j\frac{t^2}{2\ddot{\Phi}}\right) = \int_{-\infty}^{\infty} g(\tau) \times \exp\left[j\frac{(t-\tau)^2}{2\ddot{\Phi}}\right] d\tau \tag{13}$$

$$= \exp\left(j\frac{t^2}{2\ddot{\Phi}}\right) \times \int_{-\infty}^{\infty} g(\tau) \times \exp\left(j\frac{\tau^2}{2\ddot{\Phi}}\right) \times \exp\left[-j\left(\frac{t}{\ddot{\Phi}}\right)\tau\right] d\tau$$

$$\approx \exp\left(j\frac{t^2}{2\ddot{\Phi}}\right) \times \int_{-\infty}^{\infty} g(\tau) \times \exp\left[-j\left(\frac{t}{\ddot{\Phi}}\right)\tau\right] d\tau$$

$$= \exp\left(j\frac{t^2}{2\ddot{\Phi}}\right) \times G(\omega)\Big|_{\omega=\frac{t}{\ddot{\Phi}}}$$

where $G(\omega)$ is the Fourier transform of $g(t)$.

As can be seen the output signal envelope is proportional to the Fourier transform of the input signal envelope. Note that Eq. (13) is obtained if the duration of the input ultrashort pulse, Δt_0, and the second-order dispersion $\ddot{\Phi}$ of the dispersive element satisfy the following condition,

$$\left|\frac{\Delta t_0^2}{2\ddot{\Phi}}\right| \ll 1, \tag{14}$$

which means the phase term $\frac{\tau^2}{2\ddot{\Phi}}$ in Eq. (13) satisfies $\frac{\tau^2}{2\ddot{\Phi}} \le \frac{\Delta t_0^2}{2\ddot{\Phi}} \ll 1$, thus we have $\exp\left(j\frac{\tau^2}{2\ddot{\Phi}}\right) \approx 1$ [14].

The wavelength-to-time mapping is illustrated in Fig. 4(b). If the input to the dispersive device is a rectangular pulse, then the output temporal waveform should be a sinc function. As can be seen, the key device in the arbitrary microwave waveform generator is the spectral shaper, which should be designed to have a magnitude response that can make the shaped spectrum have the same shape as the microwave waveform to be generated.

Based on this concept, a few approaches to generating chirped microwave waveforms [15–23] were demonstrated. The main effort in these approaches is to design an optical spectral shaper that has a magnitude response with its shape identical to that of the microwave waveform to be generated. Fig. 5(a) shows a spectral-shaping and wavelength-to-time mapping system for the generation of a chirped microwave waveform [17]. An ultra-short pulse from a mode-locked laser is sent to an optical spectral shaper. For chirped microwave waveform generation, the magnitude response of the optical spectral shaper should have an increasing or decreasing free spectral range (FSR) which is termed chirped FSR in [17]. The spectrum-shaped pulse is then sent to a dispersive element, which is a length of single-mode fiber (SMF), as shown in Fig. 5(a). To obtain a spectral response with a chirped FSR, the spectral shaper is designed by superimposing two chirped fiber Bragg gratings with different chirp rates into a same fiber with a small longitudinal offset, as shown in Fig. 5(b). Distributed Fabry–Perot interference is then produced in the fiber due to the reflections between the two chirped fiber Bragg gratings. This generates an in-fiber optical filter with an FSR inversely proportional to the cavity length L. Since the two chirped fiber Bragg gratings have different linear chirp rates, the equivalent cavity length L varies linearly with respect to optical wavelength λ. As a result, the FSR is not constant but is increasing or decreasing with respect to optical wavelength.

From Fig. 5(b), we can see the equivalent cavity length L is linearly proportional to the wavelength λ within the filter bandwidth,

$$L(\lambda) = d + \frac{C_1 - C_2}{C_1 C_2}(\lambda - \lambda_0) \tag{15}$$

where C_1 and C_2 are the chirp rates of the two chirped fiber Bragg gratings (in nm/mm), d is the longitudinal offset, and λ_0 is the start wavelength.

The FSR of the distributed Fabry–Perot filter is given by

$$FSR \cong \frac{\lambda_0^2}{2n_{eff}L(\lambda)} \tag{16}$$

where n_{eff} is the effective refractive index of the fiber. After the dispersion-induced linear frequency-to-time mapping, the FSR is mapped to the temporal period of the generated chirped pulse, namely, $\Delta\tau$, with a mapping relationship $\lambda \to t/\chi$, where χ (ps/nm) is the total dispersion of the SMF.

For simplicity, the instantaneous microwave carrier frequency of the generated temporal pulse, f_{RF}, can be approximated by the reciprocal of the temporal period $\Delta\tau$.

$$f_{RF}(t) = \frac{1}{\Delta\tau} = 2n_{eff}\left[\frac{C_1 - C_2}{C_1 C_2} \times \left(\frac{t}{\lambda_0^2\chi^2} - \frac{1}{\lambda_0\chi}\right) + \frac{d}{\lambda_0^2\chi}\right] \tag{17}$$

It can be seen that the frequency of the microwave waveform is linearly proportional to time t, therefore the generated microwave waveform is linearly chirped. For the SMF with a given length, the central carrier frequency of the generated chirped pulse at $t=0$ is dependent only upon the longitudinal offset d. The chirp rate of the generated pulse is determined by the chirp rates of the two chirped fiber Bragg gratings. Therefore, by choosing the longitudinal offset and the chirp rates of the chirped fiber Bragg gratings, a linearly chirped microwave waveform with a high central frequency and a large chirp rate can be generated.

The major limitation of the approach in [17] is that the optical spectral shaper, once fabricated, is not reconfigurable. For many applications, however, it is expected that the chirp rate and the center frequency of the microwave chirped waveform can be tunable. To solve

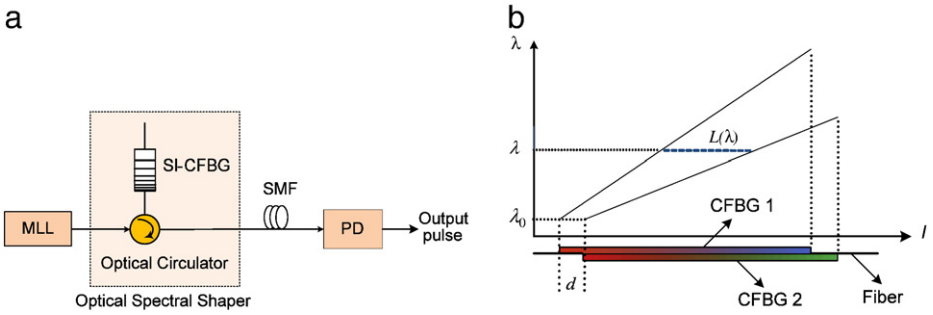

Fig. 5. Chirped microwave waveform generation based on spectral-shaping and wavelength-to-time mapping. (a) Schematic of the chirped microwave pulse generation system. (b) Optical spectral shaper consisting of two superimposed chirped fiber Bragg gratings with different chirp rates and a small longitudinal offset. MLL: mode-locked laser; SI-CFBG: superimposed chirped fiber Bragg grating; SMF: single mode fiber; PD: photodetector.

this problem, we proposed an optical spectral shaper that is a Sagnac-loop mirror incorporating a chirped fiber Bragg grating [18]. Similar to the superimposed chirped fiber Bragg gratings in [17], due to the incorporation of a chirped fiber Bragg grating, the Sagnac-loop mirror would have a distributed Fabry–Perot interference due to the reflections from the two opposite directions of the chirped fiber Bragg grating. Thus, an in-fiber optical filter with an FSR that is inversely proportional to the length difference would be formed. Since the reflection point is wavelength dependent, the equivalent length difference varies linearly with respect to optical wavelength λ. As a result, the FSR is not constant but is increasing or decreasing with respect to the optical wavelength.

Fig. 6 shows the optical spectral shaper based on an all-fiber Sagnac-loop mirror incorporating a chirped fiber Bragg grating [18]. The Sagnac-loop mirror is constructed from a fused 3-dB fiber coupler spliced to the terminals of the chirped fiber Bragg grating, which is located approximately at the middle point of the fiber loop. A tunable delay-line (TDL) is located in the fiber loop to finely tune the time-delay difference between two fiber lengths L_1 and L_2. A polarization controller (PC) is also placed in the loop to optimize the visibility of the interference pattern at the output of the loop mirror. A three-port optical circulator is used to direct the ultrashort pulse into the loop mirror and to output the spectrum-shaped pulse for wavelength-to-time mapping.

Mathematically, the Sagnac-loop mirror incorporating a chirped fiber Bragg grating can be modeled as a two-tap delay-line filter. The transfer function of the Sagnac-loop mirror is expressed as

$$T(\lambda) = \frac{1}{2}W(\lambda)\left[1 + \cos\left(\frac{2\pi n_{eff}}{\lambda} 2\Delta L\right)\right], \left(|\lambda - \lambda_0| \le \frac{B_\lambda}{2}\right) \tag{18}$$

where $W(\lambda)$ is the intensity reflection spectrum of the chirped fiber Bragg grating with a bandwidth B_λ, and n_{eff} is the effective refractive index of the fiber core. $\Delta L = L_1 - L_2$ is the fiber length difference, with L_1 and L_2 measured from the center of the chirped fiber Bragg grating to the fiber coupler along the clockwise and counterclockwise paths as shown in Fig. 6. The fiber length difference ΔL comes from two sources: the wavelength-independent path difference, ΔL_0, and the wavelength-dependent fiber length difference introduced by the chirp of the chirped fiber Bragg grating, $\Delta L(\lambda)$. ΔL_0 can be controlled to be either a positive or a negative value by tuning the TDL in the fiber loop. $\Delta L(\lambda)$ is determined by the bandwidth and the chirp parameter of the chirped fiber Bragg grating, and can be calculated using $\Delta L(\lambda) = \delta\lambda / C$, where $\delta\lambda$ (nm) is the wavelength detuning from the center wavelength λ_0, and C (nm/cm) is the chirp parameter of the chirped fiber Bragg grating. Then the filter transfer function $T(\lambda)$ can be rewritten as

$$T(\lambda) = \frac{1}{2}W(\lambda)\left\{1 + \cos\left[\frac{4\pi n_{eff}}{\lambda_0^2}\lambda\left(\Delta L_0 + \frac{\delta\lambda}{C}\right)\right]\right\}. \tag{19}$$

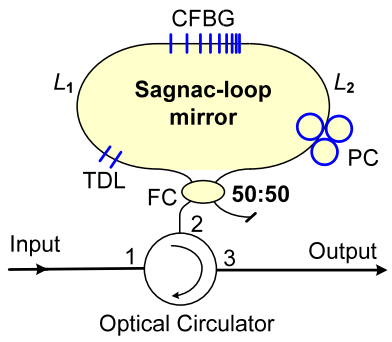

Fig. 6. An all-fiber optical spectral shaper consisting of Sagnac-loop mirror incorporating a chirped fiber Bragg grating. FC: fiber coupler; TDL: tunable delay-line; CFBG: chirped fiber Bragg grating; PC: polarization controller.

Since the linearly chirped fiber Bragg grating is located in the fiber loop, an optical signal with different wavelengths will be reflected from a different position in the chirped fiber Bragg grating. As a result, an optical spectral filter with a wavelength-dependent FSR is formed. The FSR of the optical spectral filter response is a function of the wavelength and can be expressed as

$$FSR = \frac{\lambda^2}{2n_{eff}|\Delta L|} = \frac{\lambda_0^2}{2n_{eff}\left|\frac{\delta\lambda}{C} + \Delta L_0\right|} \tag{20}$$

According to Eq. (20), by properly choosing the parameters of the chirped fiber Bragg grating and by controlling the TDL in the fiber loop, the FSR of the Sagnac-loop mirror can be controlled.

After the spectrum-shaped optical pulse propagates through the dispersive element and is detected by the high-speed PD, the shaped spectrum is mapped into a temporal microwave pulse as $T(\lambda) \to y(t)$ thanks to the dispersion-induced linear wavelength-to-time mapping. Assume that the input ultrashort optical pulse is a unit impulse, according to the mapping relationship $\lambda \to t/\chi$, the time-domain waveform is given by

$$y(t) = \frac{1}{2}W\left(\frac{t}{\chi}\right)\left\{1 + \cos\left[\frac{4\pi n_{eff}}{\lambda_0^2\chi}t\left(\Delta L_0 + \frac{\delta t}{C\chi}\right)\right]\right\} \tag{21}$$

where δt is the time detuning from the center of the temporal waveform, which is given by the mapping relationship $\delta\lambda \to \delta t/\chi$. The time-domain pulse duration ΔT of the generated microwave pulse is determined by the window function $W(t/\chi)$, and is calculated by $\Delta T = B_\lambda\chi$. Considering that the pulse width of the input ultrashort optical pulse is not zero, the detected pulse envelope should be modified by adding an envelope $r(t)$,

$$y(t) = \frac{1}{2}r(t)W\left(\frac{t}{\chi}\right)\left\{1 + \cos\left[\frac{4\pi n_{eff}}{\lambda_0^2\chi}t\left(\Delta L_0 + \frac{\delta t}{C\chi}\right)\right]\right\} \tag{22}$$

where $r(t)$ is the pulse envelope after the input pulse passing through the dispersive element. Assuming that the input ultrashort optical pulse has a Gaussian envelope as $g(t) \propto \exp(-t^2/\Delta t_0^2)$, where Δt_0 is the half pulse-width at 1/e maximum, then the envelope of output pulse from a dispersive element will maintain the Gaussian shape, but with a broadened pulse width of $|\ddot{\Phi}| / \Delta t_0$. Actually, the envelope $r(t)$ is a scaled version of the spectrum envelope of the input pulse, which is mapped to the time domain thanks to the dispersion-induced frequency-to-time mapping in the chirped fiber Bragg grating.

The instantaneous microwave carrier frequency of the generated waveform can be obtained from the phase term of Eq. (22), which is expressed as

$$f_{RF}(\delta t) = \frac{1}{2\pi} \times \frac{d\Psi}{dt} = \frac{2n_{eff}}{\lambda_0^2\chi}\left(|\Delta L_0| \pm \frac{\delta t}{C\chi}\right). \tag{23}$$

It is shown that the generated microwave waveform is linearly chirped. For a given dispersive element, the central microwave carrier frequency of the generated chirped microwave pulse is only determined by the absolute value of wavelength-independent fiber length difference ΔL_0. Therefore, the central frequency of the generated microwave chirped waveform can be tuned by simply tuning ΔL_0. The chirp rate of the generated microwave waveform, given by

$$CR_{RF} = df_{RF}(\delta t) / d\delta t = \pm 2n_{eff} \Big/ \left(C\lambda_0^2\chi^2\right), \tag{24}$$

is only dependent on the dispersion of the chirped fiber Bragg grating. The sign of the chirp rate corresponds to the positive and negative values of ΔL_0. Therefore, by appropriately controlling the TDL and choosing the

dispersion of the chirped fiber Bragg grating, a linearly chirped microwave pulse with a high central frequency and a tunable chirp rate can be generated. Fig. 7 shows the spectra of a Gaussian pulse after spectral shaping by the Sagnac-loop mirror for different ΔL_0. The corresponding temporal domain waveforms after wavelength-to-time mapping are also shown.

In [17] and [18], the spectral shaper for spectrum shaping and the dispersive element for wavelength-to-time mapping are two separate components. In fact, the two components can be a single component if the magnitude response and the group delay response can be individually controlled to perform simultaneously spectrum shaping and wavelength-to-time mapping. In [19], a single chirped fiber Bragg grating was employed to perform the two functions, as shown in Fig. 8(a).

The key component in the system is the linearly chirped fiber Bragg grating, which should be designed to have a magnitude as well as a group delay response that can fulfill the requirements for both spectral shaping and wavelength-to-time mapping. Different techniques have been proposed to synthesize an FBG, such as the well-known discrete layer-peeling (DLP) algorithm [24–26] and the Gelfand–Levitan–Marchenko (GLM) inverse scattering algorithm [27].

Here a simplified approach is employed to synthesize the LCFBG [19]. Fig. 8(b) shows the magnitude and the group delay response of a linearly chirped fiber Bragg grating. The magnitude response has an increasing FSR and the group delay response is linear. Thanks to the inherent linear group delay response, a linearly chirped fiber Bragg

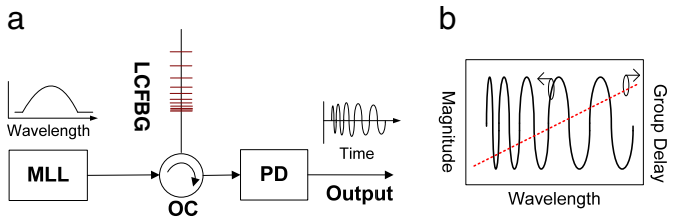

Fig. 8. (a) A microwave arbitrary waveform generator basd on spectral-shaping and wavelength-to-time mapping using a single linearly chirped fiber Bragg grating. (b) The magnitude and phase responses of the linearly chirped fiber Bragg grating. MLL: mode-locked laser, LCFBG: linearly chirped fiber Bragg grating, PD: photodetector.

grating can always act as a linear wavelength-to-time mapper. Therefore, the focus of the work is to synthesize the grating refractive index modulation profile from the target grating magnitude response. The synthesis is performed based on an accurate mapping of grating reflection response to the refractive index modulation [19]. We can first set up the mapping relationship by applying a linearly increasing index modulation function to a test grating with the use of a linearly chirped phase mask and then measuring the grating reflection spectrum. A linear index modulation function is first constructed, which is expressed as

$$\Delta n_L(z) = \Delta n_{\max}\frac{z}{L}\exp\left(j\frac{2\pi z}{\Lambda_0}\right)\exp\left[-j\frac{2\pi C(z-L/2)^2}{\Lambda_0^2}\right] \tag{25}$$

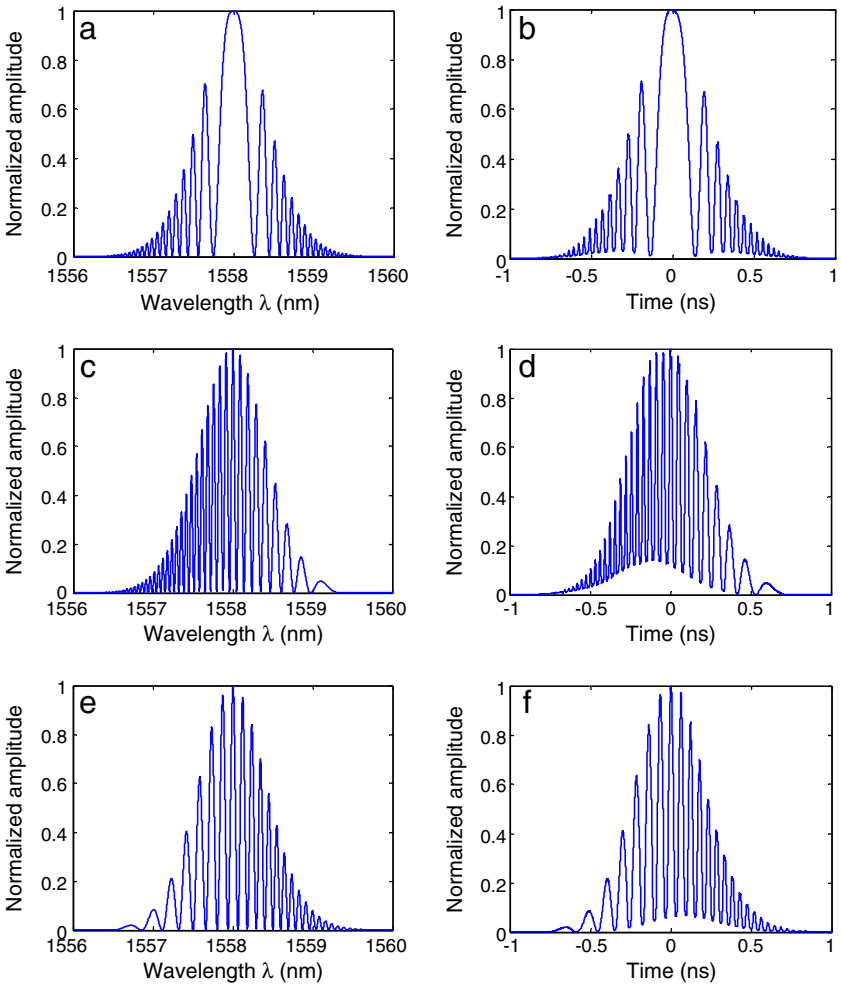

Fig. 7. The spectra of an optical Gaussian pulse after spectral shaping by the Sagnac-loop mirror and the corresponding temporal waveforms. (a) A symmetrical FSR ($\Delta L_0 = 0$), (c) an increasing FSR ($\Delta L_0 = -9.7$ mm), and (e) a decreasing FSR ($\Delta L_0 = 6.9$ mm). The generated time-domain waveforms with (b) a symmetrical chirp rate and a zero central frequency, (d) a negative chirp rate and a central frequency of 22.3 GHz, and (f) a positive chirp rate and a central frequency of 16.1 GHz.

where Λ_0 is the grating period at the center of the linearly chirped fiber Bragg grating, L is the length of the linearly chirped fiber Bragg grating, and C is the grating chirp rate. We can imprint the index modulation function in Eq. (25) into the test grating using a given linearly chirped phase mask. Then the reflection spectrum $R_{test}(\lambda)$ of the fabricated test grating is measured. By equally dividing the grating into N consecutive segments with positions z_i ($1 \le i \le N$), we can get the sampled reflection spectrum $R_{test}(\lambda_i)$ thanks to the unique mapping relationship between $\Delta n_L(z_i)$ and $R_{test}(\lambda_i)$.

For a grating with a target reflection spectrum $R_{tgt}(\lambda)$, we can compare it with the test grating response $R_{test}(\lambda_i)$ wavelength by wavelength and then determine the desired index modulation function $\Delta n_D(z_i)$ by querying the linear index modulation function $\Delta n_L(z_i)$ segment by segment. Therefore, by applying the amplitude-only index modulation $\Delta n_D(z_i)$ under the same experimental condition, a desired linearly chirped fiber Bragg grating with the target reflection spectrum can be easily fabricated with the current FBG fabrication technology.

To improve the reconfigurability, recently an integrated arbitrary microwave waveform generator that incorporates a fully-programmable spectral shaper fabricated on a silicon photonic chip was demonstrated [20]. The spectral shaper consists of a cascade of multi-channel microring resonators on a silicon photonics platform that is compatible with electronic integrated circuit technology. The system reconfigurability is achieved by thermally tuning both the resonant frequencies and the coupling strengths of the microring resonators. Two generations of the microring spectral shaper were developed. In the first generation system, the resonators have a ring structure with the central wavelength of each resonator independently tuned by a micro-heater placed above the microring, and have a tuning speed at millisecond to microsecond range. Since the heating of the ring has little impact on the coupling efficiency, which is crucial in controlling the magnitude profile of the spectral shaper, a coupler with a Mach–Zehnder structure in the input port of each microring was added in the second generation system. By thermally tuning the phase shift between the two arms, the coupling coefficient into a ring can be adjusted. It was demonstrated that for each resonant frequency, full tuning from the on state (no dip) to the off state can be achieved. By incorporating the spectral shaper into a photonic arbitrary microwave waveform generation system, a variety of different waveforms are generated including those with an apodized amplitude profile, multiple π phase shifts, two-tone waveforms and frequency-chirped waveforms [20].

More recently, we demonstrated a more flexible approach to the generation of microwave arbitrary waveforms using a single spatially discrete chirped fiber Bragg grating (SD-CFBG) [21]. The SD-CFBG functions to perform simultaneously spectral slicing, frequency-to-time mapping, and temporal shifting of the input optical pulse, which leads to the generation of an optical pulse burst with the individual pulses in the burst temporally spaced by the time delays determined by the SD-CFBG. With the help of a bandpass filter, a smooth microwave waveform is obtained. The SD-CFBG is fabricated using a linearly chirped phase mask by axially shifting the photosensitive fiber to introduce a spatial spacing between two adjacent sub-gratings during the fabrication process. By properly designing the fiber shifting function, a large time-bandwidth-product microwave arbitrary waveform with the desired frequency chirping or phase coding can be generated. The photonic generation of large TBWP microwave waveforms with a linear, nonlinear and stepped frequency chirping was experimentally demonstrated.

Instead of using a dispersive element with only the second-order dispersion for linear wavelength-to-time mapping, a dispersive element with both the second- and third-order dispersion can be used to achieve nonlinear wavelength-to-time mapping. For the case of chirped microwave waveform generation, for example, if a dispersive element with both the second- and third-order dispersion is employed, a chirped microwave waveform can be generated using an optical spectral shaper with a uniform FSR, which would simplify the implementation [22,23].

If the dispersion up to the third order is considered, then a new wavelength-to-time mapping function would be used, which is given by [28]

$$\omega = \frac{t}{\ddot{\Phi}} - \frac{\dddot{\Phi} t^2}{2\ddot{\Phi}^3}, \tag{26}$$

where $\dddot{\Phi}$ is the third-order dispersion. Assume that the spectral shaper is a Sagnac-loop filter, the transfer function of the two-tap Sagnac-loop filter is given by

$$H(\omega) = \frac{1}{2}[1 + \cos(\omega\tau_0)] \tag{27}$$

where τ_0 is the time-delay difference between the two taps. Based on wavelength-to-time mapping, a microwave waveform to be generated is given

$$i(t) = r(t) \times \frac{1}{2}\left[1 + \cos\left(\frac{t}{\ddot{\Phi}} - \frac{\dddot{\Phi} t^2}{2\ddot{\Phi}^3}\right)\tau_0\right] \tag{28}$$

where $r(t)$ is again the pulse envelope. If the input short pulse from the mode-locked laser is a Gaussian pulse, the output pulse envelope $r(t)$ can be analytically expressed using the Airy function [22].

The instantaneous microwave carrier frequency of the obtained waveform can be written as

$$\omega_{RF}(t) = \frac{d}{dt}\left(\frac{t}{\ddot{\Phi}} - \frac{\dddot{\Phi} t^2}{2\ddot{\Phi}^3}\right)\tau_0 = \frac{\tau_0}{\ddot{\Phi}} - \frac{\dddot{\Phi}\tau_0}{\ddot{\Phi}^3} t. \tag{29}$$

As can be seen, the frequency of the microwave carrier is not constant, but a function of time. The microwave waveform is linearly chirped.

4. Temporal pulse shaping

Microwave waveforms can also be generated based on temporal pulse shaping (TPS) [29–32]. A TPS system usually consists of a mode locked laser source, a pair of complementary dispersive elements and a modulator. The modulator can be a MZM [30,31] or a phase modulator [32]. Fig. 9 shows a schematic of a TPS system, in which the modulator is a MZM.

Again, if $|\Delta t_0^2/\ddot{\Phi}| \ll 1$, where Δt_0 is the temporal width of the input short pulse, the electrical field of the short pulse $g(t)$ after propagating through the first dispersive element with a dispersion of $-\ddot{\Phi}$ can be expressed as [14]

$$\begin{aligned} p(t) &= g(t) * \exp\left(j\frac{t^2}{2\ddot{\Phi}}\right) = \int_{-\infty}^{\infty} g(\tau) \times \exp\left[j\frac{(t-\tau)^2}{2\ddot{\Phi}}\right] d\tau \\ &= \exp\left(j\frac{t^2}{2\ddot{\Phi}}\right)\int_{-\infty}^{\infty} g(\tau) \times \exp\left(j\frac{t^2}{2\ddot{\Phi}}\right) \times \exp\left[j\left(-\frac{t}{\ddot{\Phi}}\right)\tau\right] d\tau \\ &\approx \exp\left(j\frac{t^2}{2\ddot{\Phi}}\right)\int_{-\infty}^{\infty} g(\tau) \times \exp\left[j\left(-\frac{t}{\ddot{\Phi}}\right)\tau\right] d\tau \\ &= \exp\left(j\frac{t^2}{2\ddot{\Phi}}\right) G(\omega)\Big|_{\omega=\frac{t}{\ddot{\Phi}}} \end{aligned} \tag{30}$$

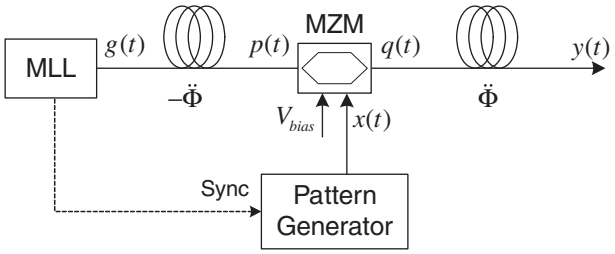

Fig. 9. Schematic a TPS system for arbitrary waveform generation.

where $G(\omega)$ is the Fourier transform of $g(t)$. The signal at the output of the MZM,

$$q(t) = p(t) \times x(t) = \exp\left(j\frac{t^2}{2\ddot{\Phi}}\right) \times G\left(\frac{t}{\ddot{\Phi}}\right) \times x(t) \tag{31}$$

where $x(t)$ is the input microwave signal to the MZM.

After propagating through the second dispersive element that has an opposite chromatic dispersion $\ddot{\Phi}$, we obtain the output temporal signal as the convolution of $q(t)$ with the impulse response of the dispersive element $\exp(-jt^2/2\ddot{\Phi})$,

$$\begin{aligned} y(t) &= q(t) * \exp\left(-j\frac{t^2}{2\ddot{\Phi}}\right) = \int_{-\infty}^{\infty} q(\tau) \times \exp\left[-j\frac{(t-\tau)^2}{2\ddot{\Phi}}\right] d\tau \\ &= \exp\left(-j\frac{t^2}{2\ddot{\Phi}}\right) \times \int_{-\infty}^{\infty} q(\tau) \times \exp\left(-j\frac{\tau^2}{2\ddot{\Phi}}\right) \times \exp\left[j\left(\frac{t}{\ddot{\Phi}}\right)\tau\right] d\tau \\ &= \exp\left(-j\frac{t^2}{2\ddot{\Phi}}\right) \times \int_{-\infty}^{\infty} \exp\left(j\frac{\tau^2}{2\ddot{\Phi}}\right) \times G\left(\frac{\tau}{\ddot{\Phi}}\right) \times x(\tau) \times \exp\left(-j\frac{\tau^2}{2\ddot{\Phi}}\right) \\ &\quad \times \exp\left[j\left(\frac{t}{\ddot{\Phi}}\right)\tau\right] d\tau = \exp\left(-j\frac{t^2}{2\ddot{\Phi}}\right) \times \int_{-\infty}^{\infty} \left[G\left(\frac{\tau}{\ddot{\Phi}}\right) \times x(\tau)\right] \\ &\quad \times \exp\left[-j\left(-\frac{t}{\ddot{\Phi}}\right)\tau\right] d\tau \\ &= \exp\left(-j\frac{t^2}{2\ddot{\Phi}}\right) \times F\left[G\left(\frac{t}{\ddot{\Phi}}\right) \times x(t)\right]\Big|_{\omega=-\frac{t}{\ddot{\Phi}}} \\ &= 2\pi|\ddot{\Phi}| \exp\left(-j\frac{t^2}{2\ddot{\Phi}}\right) \times \left[g(-t) * X\left(-\frac{t}{\ddot{\Phi}}\right)\right] \end{aligned} \tag{32}$$

where F denotes the Fourier transform operation, $*$ denotes the convolution operation, and $X(\omega)$ is the Fourier transform of $x(t)$.

As can be seen from Eq. (32) the output waveform is a convolution between the input optical pulse and the Fourier transform of the input modulation signal. If the input optical pulse is ultra short, say, a unit impulse function, the convolution of a function with a unit impulse is the function itself, then the generated waveform is simply the Fourier transform of the modulation signal. Based on the property of Fourier transform, a slow waveform would lead to the generation of a fast waveform with narrow temporal width.

The major challenge in implementing a TPS system is the complexity in the modulation stage since the modulation signal is usually complex-valued. For example, to generate a non-symmetrical waveform, based on Fourier transform property, the modulation signal is complex valued. Therefore, in the modulation stage an amplitude modulator and a phase modulator must be employed, and the magnitude and phase information must be precisely synchronized, which makes the system extremely complicated. Considering the fact that the Fourier transform of a real and symmetrical waveform is still real and symmetrical, it is possible to use an MZM that is biased at the minimum transmission point to perform temporal spectrum shaping with a real signal that has both positive and negative values [33]. With this concept, waveforms such as square waves, rectangular waves, triangular waves or doublet can be easily generated.

The TPS systems in [30–33] were employed for the generation of optical waveforms. In fact, the TPS technique can be extended for the generation of high-frequency microwave waveforms. Recently, the generation of a microwave waveform with a continuously tunable frequency by use of an unbalanced temporal pulse shaping system was proposed [34]. As can be seen from Eq. (32), in a conventional TPS system the output waveform is the Fourier transformation of the input modulation signal. If a second Fourier transformation is applied to the output waveform of a conventional TPS system, the finally generated waveform would be a scaled version of the input modulation signal. The second Fourier transformation can be performed by adding a third dispersive element, the entire system is then called an unbalanced TPS system. The schematic of the system is illustrated in Fig. 10.

In general, the values of the third-order dispersion of the two dispersive elements are small and negligible, and only the second-order dispersion or group velocity dispersion (GVD) is considered. The dispersive elements can then be characterized by the transfer function given by $H_i(\omega) = \exp(-j\ddot{\Phi}_i\omega^2/2), (i = 1, 2)$, where $\ddot{\Phi}_1$ and $\ddot{\Phi}_2$ (ps^2) are the dispersion of the two dispersive elements. In the unbalanced TPS system, the dispersion values should satisfy $\ddot{\Phi}_1\ddot{\Phi}_2 < 0$, and $|\ddot{\Phi}_1| \neq |\ddot{\Phi}_2|$. Therefore, the entire unbalanced TPS system can be modeled as a typical TPS system with a pair of complementary dispersive elements, followed by a residual dispersive element with a transfer function of $H_3(\omega) = \exp(-j\ddot{\Phi}_3\omega^2/2)$, where $\ddot{\Phi}_3 = \ddot{\Phi}_1 + \ddot{\Phi}_2$ is defined as the residual dispersion.

Mathematically, when a continuous-wave $x(t) = \exp(j\omega_m t)$ with an angular frequency of ω_m is applied to a MZM, the modulated signal $e_{IM}(t)$ at the output of the MZM is given by $e_{IM}(t) = \exp(j\omega_0 t) \times \{\exp[j\beta x(t)] + \exp[-j\beta x(t) + j\phi_0]\}$. Based on Taylor expansion, we have

$$e_{IM}(t) = \exp(j\omega_0 t) \times \left\{ \sum_{n=0}^{\infty} \frac{[j\beta x(t)]^n}{n!} + e^{j\phi_0} \sum_{n=0}^{\infty} \frac{[-j\beta x(t)]^n}{n!} \right\}, \tag{33}$$

where β is the phase modulation index, ϕ_0 is a phase shift introduced by the dc bias. To make the MZM operate at the minimum transmission point for the suppression of the optical carrier, a dc voltage is applied to the MZM to introduce a π phase shift (i.e., $\phi_0 = \pi$) between the two arms of the MZM. If the modulation index β is sufficiently small, $e_{IM}(t)$ can be approximated to be $e_{IM}(t) \approx \exp(j\omega_0 t) \times [2j\beta x(t)]$. Therefore, the modulation function of the MZM biased at the minimum transmission point is $2j\beta x(t)$.

It is known that if the first dispersive element has an adequate dispersion, i.e., $|\Delta t_0^2/\ddot{\Phi}| \ll 1$, Δt_0 is the pulse width of the input optical pulse $g(t)$, the output signal of the typical TPS system, $s(t)$, shown in Fig. 10(b), is the convolution between the input signal and the Fourier transform of the modulation function,

$$s(t) \propto g(t) * E_{IM}(\omega)|_{\omega = t/\ddot{\Phi}_1} = J_1(\beta)[g(t - T_1) + g(t + T_1)] \tag{34}$$

where $E_{IM}(\omega)$ is the Fourier transform of $e_{IM}(t)$, $*$ denotes the convolution operation, and $T_1 = |\omega_m\ddot{\Phi}_1|/2\pi$. Therefore, two time-delayed replicas of the input pulse are generated at the output of the typical TPS system, which correspond to the two optical sidebands at the output of the DSB-SC modulator.

The electrical field at the output of the entire unbalanced TPS system, $y(t)$, is obtained by propagating $s(t)$ through the residual

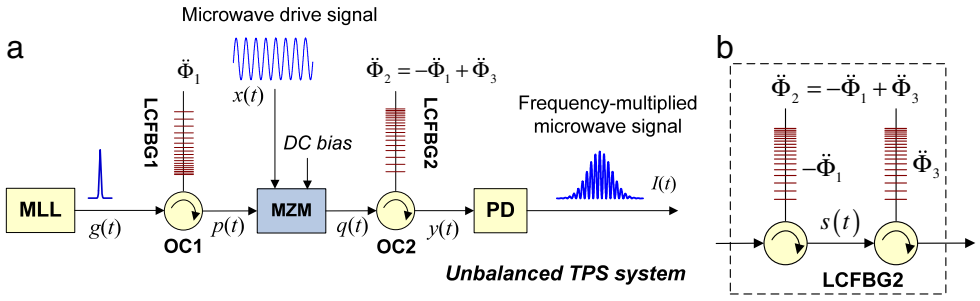

Fig. 10. (a) An unbalanced TPS system for the generation of a microwave waveform with tunable carrier frequency. (b) The second linearly chirped fiber Bragg grating can be considered as a cascade of two linearly chirped fiber Bragg gratings with the first one having the opposite dispersion to LCFBG1 and the second one having a residual dispersion.

dispersive element. If $|T_1^2/2\ddot{\Phi}_3|<<1$ is satisfied, then $y(t)$ can be approximated by the real-time FT of $s(t)$ in the residual dispersive element [34],

$$\begin{aligned} y(t) &\approx \exp\left[jt^2/\left(2\ddot{\Phi}_3\right)\right] S(\omega)|_{\omega=t/\ddot{\Phi}_3} \\ &= \exp\left[jt^2/\left(2\ddot{\Phi}_3\right)\right] J_1(\beta) G\left(t/\ddot{\Phi}_3\right) \cos\left(tT_1/\ddot{\Phi}_3\right) \end{aligned} \tag{35}$$

where $G(\omega)$ is the Fourier transform of the input pulse $g(t)$.

The current at the output of the PD is proportional to the intensity of the input electrical field, which is given by

$$I(t) = R|y(t)|^2 = K\exp\left(-\frac{t^2}{\tau^2}\right)\left[1+\cos\left(2\pi\frac{2T_1}{\ddot{\Phi}_3}t\right)\right] \tag{36}$$

where R is the responsivity of the PD, $K = RJ_1^2(\beta)\pi\Delta t_0^2/2$ is a time-independent constant, and $\tau = \sqrt{2}\Delta\ddot{\Phi}/\Delta t_0$ is the output pulse width. A frequency-multiplied microwave signal is generated, which is a pulsed microwave signal with a Gaussian envelope. The new carrier frequency is

$$\omega_{RF} = 2\pi|2T_1/\Delta\ddot{\Phi}| = \omega_m|2\ddot{\Phi}_1/\ddot{\Phi}_3| \tag{37}$$

From Eq. (37) we can conclude that the frequency multiplication factor $M = \omega_{RF}/\omega_m = 2|\ddot{\Phi}_1/\ddot{\Phi}_3|$ is determined by both the stretching dispersion $\ddot{\Phi}_1$ and the residual dispersion $\ddot{\Phi}_3$. Fig. 11 shows the simulation results of an unbalanced TPS system for the generation of a microwave waveform with tunable carrier frequency. Note that the MZM in the unbalanced TPS system is biased at the minimum transmission point to suppress the optical carrier. If the MZM is biased

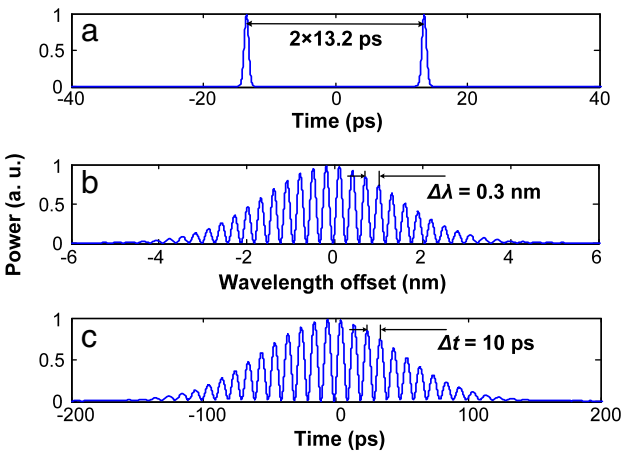

Fig. 11. Simulation results. (a) Signal at the output of the typical TPS system. (b) The optical spectrum of the signal in (a). (c) The frequency-multiplied microwave signal at the output of the entire system.

at the quadrature point, double-sideband modulation would be resulted. The use of double-sideband modulation would cause the dispersion-induced power cancelation, leading to a reduced fringe visibility, as shown in Fig. 12.

If the dispersion up to the third order is considered, then a new wavelength-to-time mapping function would be used, which is given in Eq. (26), then, the signal $q(t)$ at the output of the MZM is given by

$$q(t) = e_{\mathrm{IM}}(t)\times G(\omega)\Big|_{\omega=\frac{t}{\ddot{\Phi}_1}-\frac{\dddot{\Phi}_1 t^2}{2\ddot{\Phi}_1^3}} = [2j\beta x(t)]\times G(\omega)\Big|_{\omega=\frac{t}{\ddot{\Phi}_1}-\frac{\dddot{\Phi}_1 t^2}{2\ddot{\Phi}_1^3}}. \tag{38}$$

Since the first and second dispersive elements have conjugate dispersion and the third-order dispersion of the dispersive element is very small, the signal $s(t)$ at the output of the second dispersive element, shown in Fig. 10(b), is given by

$$s(t) = F[q(t)]\Big|_{\omega=\frac{t}{\ddot{\Phi}_2}-\frac{\dddot{\Phi}_2 t^2}{2\ddot{\Phi}_2^3}} = \frac{2j\beta}{|\ddot{\Phi}_2|}\times g(t)*X(\omega)\Big|_{\omega=\frac{t}{\ddot{\Phi}_2}-\frac{\dddot{\Phi}_2 t^2}{2\ddot{\Phi}_2^3}}, \tag{39}$$

with its spectrum $S(\omega)$ given by

$$S(\omega) = 2j\beta G(\omega)\times x\left(\ddot{\Phi}_2\omega + \frac{\dddot{\Phi}_2\omega^2}{2}\right). \tag{40}$$

The output signal in the frequency domain is given by

$$Y(\omega) = P(\omega)\times H_3(\omega) = P(\omega)\times\exp\left[-j\left(\frac{\ddot{\Phi}_3\omega^2}{2}+\frac{\dddot{\Phi}_3\omega^3}{6}\right)\right] \tag{41}$$

where $H_3(\omega)$ is the transfer function of the residual dispersive element, $\ddot{\Phi}_3$ and $\dddot{\Phi}_3$ are the second-order and the third-order dispersion of the residual dispersive element.

By using the nonlinear wavelength-to-time mapping function given in Eq. (26), the output signal in the time domain is given by

$$y(t) = F[s(t)]\Big|_{\omega=\frac{t}{\ddot{\Phi}_3}-\frac{\dddot{\Phi}_3 t^2}{2\ddot{\Phi}_3^3}} \propto G(\omega)x\left(\ddot{\Phi}_2\omega+\frac{\dddot{\Phi}_2\omega^2}{2}\right)\Big|_{\omega=\frac{t}{\ddot{\Phi}_3}-\frac{\dddot{\Phi}_3 t^2}{2\ddot{\Phi}_3^3}}. \tag{42}$$

If the optical signal at the output of the third dispersive element is applied to a PD, we have the output current, given by

$$\begin{aligned} i(t) &= R|y(t)|^2 \propto [G(\omega)]^2\left[x\left(\ddot{\Phi}_2\omega+\frac{\dddot{\Phi}_2\omega^2}{2}\right)\right]^2\Big|_{\omega=\frac{t}{\ddot{\Phi}_3}-\frac{\dddot{\Phi}_3 t^2}{2\ddot{\Phi}_3^3}} \\ &= \pi\tau_0^2\exp\left[-\frac{\tau_0^2}{4}\left(\frac{t}{\ddot{\Phi}_3}-\frac{\Phi_3 t^2}{2\ddot{\Phi}_3^3}\right)^2\right] \\ &\times\left[x\left(\frac{\ddot{\Phi}_2 t}{\ddot{\Phi}_3}-\frac{\ddot{\Phi}_2\dddot{\Phi}_3 t^2}{2\ddot{\Phi}_3^3}+\frac{\dddot{\Phi}_2}{2}\left(\frac{t^2}{\ddot{\Phi}_3^2}-\frac{\dddot{\Phi}_3 t^3}{\ddot{\Phi}_3^4}+\frac{\dddot{\Phi}_3^2 t^4}{4\ddot{\Phi}_3^6}\right)\right)\right]^2, \end{aligned} \tag{43}$$

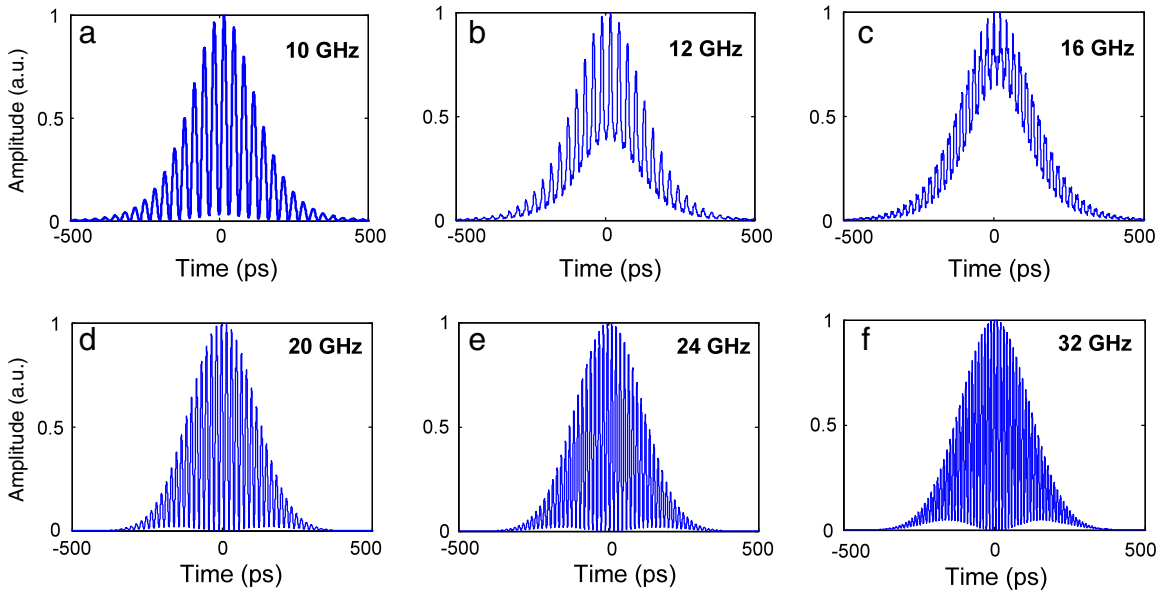

Fig. 12. Simulated output microwave waveforms based on double-sideband modulation with a carrier frequency of (a) 10 GHz, (b) 12 GHz, and (c) 16 GHz. and DSB-SC modulation with a carrier frequency of (d) 20 GHz, (e) 24 GHz, and (f) 32 GHz.

where R is again the responsivity of the PD. Usually, the third-order dispersion, $\dddot{\Phi}$, is much smaller than the second-order dispersion $\ddot{\Phi}$, and the condition $\left|T_1^2/2\dddot{\Phi}_3\right|<<1$ should be satisfied in the system where $T_1=\left|\omega_m\ddot{\Phi}_1\right|/2\pi$, we also have $\frac{t^2}{\ddot{\Phi}_3^2}>>\frac{\dddot{\Phi}_3 t^3}{\ddot{\Phi}_3^4}$ and $\frac{t^2}{\ddot{\Phi}_3^2}>>\frac{\dddot{\Phi}_3^2 t^4}{4\ddot{\Phi}_3^6}$, Eq. (43) is then simplified to

$$i(t)\propto\exp\left[-\frac{\tau_0^2}{4}\left(\frac{t}{\ddot{\Phi}_3}-\frac{\dddot{\Phi}_3 t^2}{2\ddot{\Phi}_3^3}\right)^2\right]\times\left\{x\left[\frac{\ddot{\Phi}_2}{\ddot{\Phi}_3}t+\left(\frac{\ddot{\Phi}_2\dddot{\Phi}_3-\ddot{\Phi}_2\,\ddot{\Phi}_3}{2\ddot{\Phi}_3^3}\right)t^2\right]\right\}^2. \tag{44}$$

To generate a chirped microwave pulse, we assume that the microwave modulation signal applied to the MZM is also a sinusoidal waveform with a frequency of ω_m, and the third-order dispersion of the three dispersive elements cannot be ignored. It can be seen from Eq. (44) that the output signal is also a product of a Gaussian-like function with a chirped microwave waveform. Since the angular frequency should be kept positive, the instantaneous angular frequency of the chirped microwave waveform is approximately given as

$$\omega_{RF}\cong 2\omega_m\left|\frac{\ddot{\Phi}_2}{\ddot{\Phi}_3}+\left(\frac{\ddot{\Phi}_2\dddot{\Phi}_3-\ddot{\Phi}_2\,\ddot{\Phi}_3}{\ddot{\Phi}_3^3}\right)t\right|. \tag{45}$$

Eq. (45) shows that a chirped microwave waveform can be generated if both the second and the third dispersive elements have non-zero third-order dispersion. The chirp rate is given by

$$CR_{RF}=2\omega_m\left(\frac{\ddot{\Phi}_2\dddot{\Phi}_3-\ddot{\Phi}_2\,\ddot{\Phi}_3}{\ddot{\Phi}_3^3}\right)\times sgn\left(\frac{\ddot{\Phi}_2}{\ddot{\Phi}_3}\right) \tag{46}$$

where sgn is a sign function. From Eq. (46), it can be seen that the chirp rate is determined by the values of the third-order dispersion $\dddot{\Phi}_2$ and $\dddot{\Phi}_3$. When $t=0$, the frequency is the central frequency of the generated microwave waveform which is also equal to the angular frequency ω_{RF} in Eq. (37). Therefore, a microwave waveform with a tunable central frequency and chirp rate can be generated by tuning the second-order dispersion and third-order dispersion of the second and third dispersive elements. By varying the third-order dispersion of a non-linearly chirped FBG (NLC-FBG) based on a strain-gradient beam tuning technique, the chirp rate can be continuously tunable. On the other hand, if the frequency chirp in the generated microwave waveform is not desired, the frequency chirp can be made zero by tuning the dispersion to make $\left(\ddot{\Phi}_2\dddot{\Phi}_3-\ddot{\Phi}_2\,\ddot{\Phi}_3\right)$ equal to zero.

Fig. 13 shows the experimental results of an unbalanced TPS system for the generation of microwave waveform without and with chirp [35]. In the experiment, the input microwave waveform is 1.3 GHz and the first dispersive element is a dispersion compensating fiber (DCF) with a dispersion value of $-485.07\,ps^2$. A chirped fiber Bragg grating glued on a cantilever beam was employed in the system connected to the output of the MZM. When no force is applied to the cantilever beam, the total second-order dispersion and third-order dispersion after the MZM are $-485.07\,ps^2$ and $3.34\,ps^3$. Since the unbalanced TPS system is a linear time-invariant system, the values of the second-order dispersion of the three dispersive elements in the entire system are $\ddot{\Phi}_1=772.62\,ps^2$, $\ddot{\Phi}_2=-772.62\,ps^2$, and $\ddot{\Phi}_3=287.54\,ps^2$. Based on $M=\omega_{RF}/\omega_m=2\left|\ddot{\Phi}_1/\Delta\ddot{\Phi}\right|$, the multiplication factor is calculated to be 5.38. Since the frequency of the input microwave waveform is 1.3 GHz, the central frequency of the generated microwave waveform should be 6.99 GHz. In addition, the values of the third-order dispersion of the three dispersive elements in the entire system are $\dddot{\Phi}_1=-4.44\,ps^3$, $\dddot{\Phi}_2=4.44\,ps^3$, and $\dddot{\Phi}_3=-1.09\,ps^3$. The generated microwave waveform is shown in Fig. 13(a). The central frequency is measured to be 6.75 GHz, as shown in Fig. 13(c), which agrees well with the theoretically calculated value of 6.99 GHz. Since the third-order dispersion after the MZM is $-1.09\,ps^3$, according to Eq. (46), the chirp rate is calculated to be -4.75×10^{-2} GHz/ns which is close to the chirp rate of -5.35×10^{-2} GHz/ns estimated from the generated waveform shown in Fig. 13(a).

When a force is applied to the cantilever beam, the values of the second-order dispersion and the third-order dispersion after the MZM are $-517.02\,ps^2$ and $-2.81\,ps^3$. The values of the second-order dispersion of the three dispersive elements in the entire system are $\ddot{\Phi}_1=772.62\,ps^2$, $\ddot{\Phi}_2=-772.62\,ps^2$, $\ddot{\Phi}_3=255.61\,ps^2$. Again, the MF is calculated to be 6.04. Since the frequency of the input microwave waveform is 1.3 GHz, a central frequency of the generated microwave waveform should be 7.85 GHz. The central frequency of the generated waveform estimated from the waveform shown in Fig. 13(b) is 7.5 GHz, which is close to the theoretical value of 7.85 GHz. The values of the third-order dispersion of the three dispersive elements in the

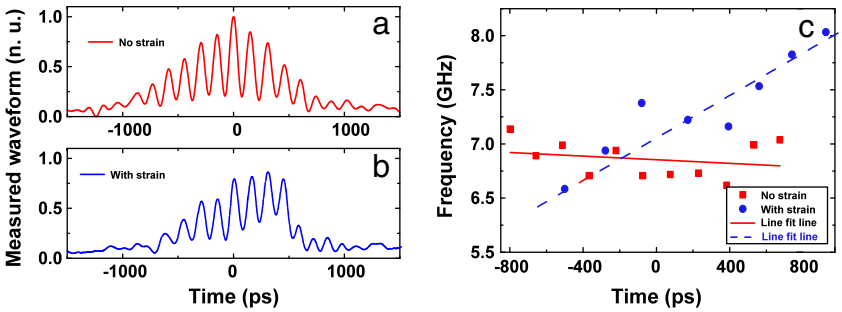

Fig. 13. Measured microwave waveforms for a unbalanced system using a chirped FBG that is glued on a cantilever beam (a) with no strain, (b) with strain, and (c) the corresponding frequency chirps with and without mechanical force applied to the free end of the cantilever beam.

entire system are $\dddot{\Phi}_1 = -4.44\,\mathrm{ps}^3$, $\dddot{\Phi}_2 = 4.44\,\mathrm{ps}^3$, $\dddot{\Phi}_3 = 5.75\,\mathrm{ps}^3$. The chirp rate calculated based on Eq. (46) is 0.868 GHz/ns, which is close to the chirp rate of 0.715 GHz/ns obtained from the generated chirped waveform shown in Fig. 13(b). In addition, the chirp rate of the experimentally generated microwave waveform is also reversed due to the change of the sign of the third-order dispersion, as shown in Fig. 13(c).

5. Microwave waveform generation based on a photonic microwave delay-line filter

The implementation of microwave delay-line filters has been a topic of interest in the last two decades [36,37]. To avoid optical interferences which are extremely sensitive to environmental changes, a photonic microwave delay-line filter is usually implemented in the incoherent regime based on incoherent detection. The major limitation of an incoherent microwave delay-line filter is that the tap coefficients are all positive, which would limit the filter to operate as a low-pass filter only. Numerous techniques have been proposed to implement a microwave delay-line filter with negative coefficients, including the use of differential detection [38], biasing a pair of MZMs at the opposite slopes [39], cross-gain modulation in a semiconductor amplifier [40], polarization modulation [41], and phase-modulation to intensity-modulation conversion [42]. A comprehensive overview of these techniques can be found in [43]. The use of a microwave delay-line filter for the generation of UWB impulse waveform has been demonstrated [44–47].

However, all the filters implemented based on the techniques in [38–42], including the filters for the generation UWB waveforms [44–47], have a linear group delay response. For microwave waveform generation, such as the generation of a chirped microwave waveform, a group delay response that is nonlinear is usually required. It is known for a delay-line filter with nonlinear group delay response, the filter should have tap coefficients that are complex, which is extremely difficult to implement especially for a filter with many taps [48–50]. Recently, we demonstrated a new concept to implement a microwave delay-line filter with arbitrary group delay response based on a delay-line structure with nonuniformly spaced taps [51]. We theoretically proved that a filter with an arbitrary frequency response in a specific resonance band can be achieved by introducing additional time delays to the taps, making the taps nonuniformly spaced.

It is known that a regular, uniformly-spaced microwave delay-line filter has an impulse response $h_0(t)$ given by

$$h_0(t) = \sum_{k=0}^{N-1} \alpha_k \delta(t-kT) \tag{47}$$

where N is the tap number, α_k is the tap coefficient of the kth tap, $T = 2\pi/\Omega$ is the time-delay difference between two adjacent taps, and Ω is the FSR of the filter. The expression of $h_0(t)$ can be expressed in another form

$$h_0(t) = a(t)s_0(t) \tag{48}$$

where $a(t)$ is the coefficient profile which can be complex valued,

$$\alpha_k = a(kT) \text{ and } a(t) = 0 \text{ if } t<0 \text{ or } t \geq NT \tag{49}$$

and $s(t)$ is the sampling function given by

$$s(t) = \sum_k \delta(t-kT). \tag{50}$$

Apply the Fourier Transfer to Eq. (47), we have the frequency response of the filter,

$$H_0(\omega) = \sum_{k=0}^{N-1} \alpha_k \exp\left(-jk\frac{2\pi}{\Omega}\omega\right). \tag{51}$$

It is known that $H_0(\omega)$ has a multi-channel frequency response with adjacent channels separated by an FSR, with the mth channel located at $\omega = m\Omega$.

In a regular photonic microwave delay-line filter based on incoherent detection, the coefficients are usually all positive, or special designs have to be incorporated to generate negative or complex coefficients [43]. However, a phase term can be introduced to a specific coefficient by adding an additional time delay at the specific tap, which is termed time-delay-based phase shift [51]. For example, at $\omega = m\Omega$ a time-delay shift of $\Delta\tau$ will generate a phase shift given by $\Delta\varphi = -\Delta\tau \times m\Omega$. Note that such a phase shift is frequency-dependent, which is accurate only for the frequency at $m\Omega$, but approximately accurate for a narrow frequency band at around $m\Omega$. For most of the applications, the filter is designed to have a very narrow frequency band. Therefore, for the frequency band of interest, the phase shift can be considered constant over the entire bandwidth. As a result, if the mth bandpass response, where $m \neq 0$, is considered, one can then achieve the desired phase shift at the kth tap by adjusting the time-delay shift by $\Delta\tau_k$. Considering the time-delay shift of $\Delta\tau_k$, one can get the frequency response of the nonuniformly-spaced delay-line filter at around $\omega = m\Omega$,

$$\begin{aligned} H_N(\omega) &= \sum_{k=0}^{N-1} \alpha_k \exp\left[-j\left(k\frac{2\pi}{\Omega} + \Delta\tau_k\right)\omega\right] \\ &= \sum_{k=0}^{N-1} \alpha_k \exp\left(-j\omega\Delta\tau_k\right) \times \exp\left(-jk\frac{2\pi}{\Omega}\omega\right) \\ &\approx \sum_{k=0}^{N-1} [\alpha_k \exp(-jm\Omega\Delta\tau_k)] \times \exp\left(-jk\frac{2\pi}{\Omega}\omega\right). \end{aligned} \tag{52}$$

As can be seen from Eq. (52), one can get an equivalent phase shift for each tap coefficient. Specifically, if the desired phase shift for the kth tap is φ_k, the total time delay τ_k for the kth tap is $\tau_k = kT - \varphi_k/m\Omega$. As a result, if the time delay of each tap is adjusted, the filter coefficients would have the required phase shifts to generate the required passband with the desired bandpass characteristics.

For a nonuniformly spaced delay-line filter with a spectral response at the $m\Omega$ that is identical to that of a regular delay-line filter with a coefficient profile given by $a(t)$, the time delays and the coefficients can be calculated by [52]

$$\tau_k + \frac{\varphi(\tau_k)}{m\Omega} = kT \tag{53a}$$

$$\beta_k = \left| \frac{a(\tau_k)}{1 + \varphi'(\tau_k)/m\Omega} \right| \tag{53b}$$

where $\varphi(t)$ is the phase term of $a(t)$. As can be seen to realize the desired bandpass response, if a regular delay-line filter is used, the tap coefficients are determined by Eq. (49), which may be negative or complex valued; however, if a nonuniformly spaced delay-line filter is used, the time delays and the tap coefficients are determined by Eqs. (53a) and (53b), and the filter has positive-only coefficients.

Since the filter can be designed to have an arbitrary spectral response, the employment of the filter for the generation of an arbitrary microwave waveform can be realized.

Fig. 14 shows a delay-line filter for the generation of phase-coded microwave waveform [52,53]. To generate the required phase code using a delay-line filter with all positive coefficients, the filter should have nonuniformly spaced taps. The desired phase coding is implemented by adjusting the time-delay differences between the adjacent taps. According to Eq. (53a) we have

$$\tau_k = T \times \left(k - \frac{\varphi_k}{2\pi m}\right) = \left(km - \frac{\varphi_k}{2\pi}\right) T_0, k = 0, 1, 2, \ldots, N-1 \tag{54}$$

where T is the time-delay difference between two adjacent taps for a uniformly spaced filter, and T_0 is the period of the microwave carrier.

For example, for a four-tap filter we have $N = 4$. If $m = 4$ is selected, for a code pattern of $\{0, \pi, \pi, 0\}$, the time delays should be $\{0, 7/8\ T, 15/8\ T, 3\ T\}$.

As a design example, a binary phase-coded microwave signal with a 13-chip Barker code, [+1, +1, +1, +1, +1, −1, −1, +1, +1, −1, +1, −1, and +1], is generated [52]. The Barker codes are usually used in direct-sequence spread-spectrum communications systems and pulse compression radar systems thanks to the excellent correlation performance. In the design, the carrier frequency is 40 GHz and $m = 4$, i.e., the chip rate is 10 GHz, and T_0 is 25 ps. Based on Eq. (54), the time delays of all the taps are calculated which are given [0, 4, 8, 12, 16, 19.5, 23.5, 28, 32, 35.5, 40, 43.5, and 48]×25 ps. If the input microwave signal is a super-Gaussian pulse with a FWHM of 100 ps, the output of the filter is calculated which is shown in Fig. 15.

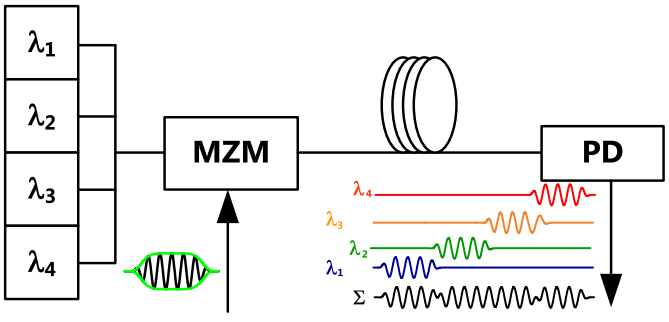

Fig. 14. A photonic microwave delay-line filter for microwave phase coding.

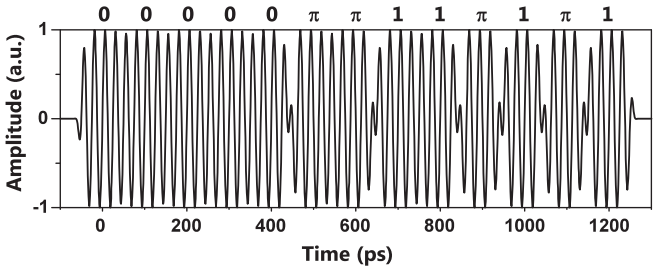

Fig. 15. Phase-coded microwave pulse with a 13-chip Barker code generated by a nonuniformly spaced delay-line filter.

A chirped microwave waveform can also be generated by using a non-uniformly spaced delay-line filter [52,54]. If a broadband chirp-free microwave pulse is passing through a microwave delay line filter with a quadratic phase response or equivalently, a linear group-delay response, a pulse burst with increasing or decreasing pulse spacing is generated. As it was proved in [12] that a pulse-position-modulated pulse burst would have a multi-channel spectral response, with one channel having a spectrum corresponding to the desired phase modulated microwave signal. By using a microwave bandpass filter to select the channel of interest, a frequency-chirped microwave signal would be generated. Fig. 16 shows a delay-line filter that can be designed to have nonuniformly spaced taps to produce a quadratic phase response. Note that instead of using an MZM, a phase modulator is employed. It was demonstrated that the phase-modulation to intensity-modulation conversion in a dispersive element will generate a notch at the dc, which is used to eliminate the resonance at the dc. The nonuniform tap spacing can be achieved in the system by tuning the wavelengths spacing. For example, if the total dispersion of the dispersive element is χ(ps/nm), then the wavelengths of the multiple wavelength sources can be calculated by

$$\lambda_k = \lambda_0 + \frac{\tau_k - \tau_0}{\chi} \tag{55}$$

where λ_0 is the wavelength for the 0th tap.

The generation of a chirped microwave pulse using a five-tap nonuniformly spaced microwave FIR filter was experimentally demonstrated. The desired pulse has an FWHM of 550 ps, a mean period of 110 ps, and a chirp rate of 13.2 GHz/ns, as shown as the dotted line in Fig. 17(a). The input pulse is a chirp-free Gaussian pulse generated in the experiment by a pattern generator with a FWHM of 65 ps. The five-tap delay line filter is designed based on (53). The time delays of the taps, calculated based on Eq. (54), are $T \times [-2.31, -1.08, 0.00, 0.81,$ and $1.51]$, where $T = 110$ ps. The wavelengths from the multi-wavelength source are then calculated based on (55). In the experiment, λ_0 is 1543.30 nm, and the five wavelengths are set as [1542.70, 1543.02, 1543.30, 1543.51, and 1543.69] nm. In the experiment, the output power of each laser is controlled such that

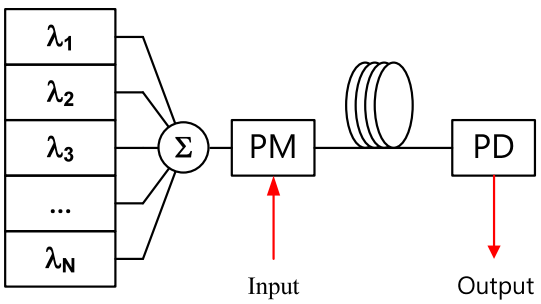

Fig. 16. A nonuniformly-spaced delay-line filter for the generation of a chirped microwave waveform. The baseband resonance is eliminated by the notch at dc due to the PM-IM conversion. PM: phase modulator. PD: photodetector.

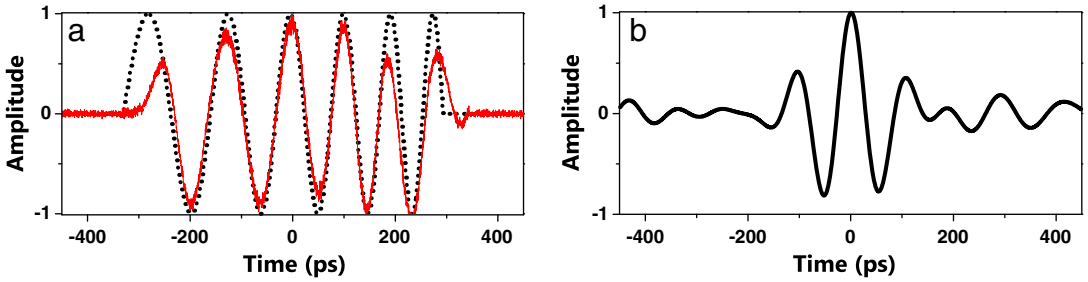

Fig. 17. (a) Solid line: the generated chirped microwave pulse. Dotted line: the desired chirped microwave pulse. (b) The correlation between the measured and the reference pulses.

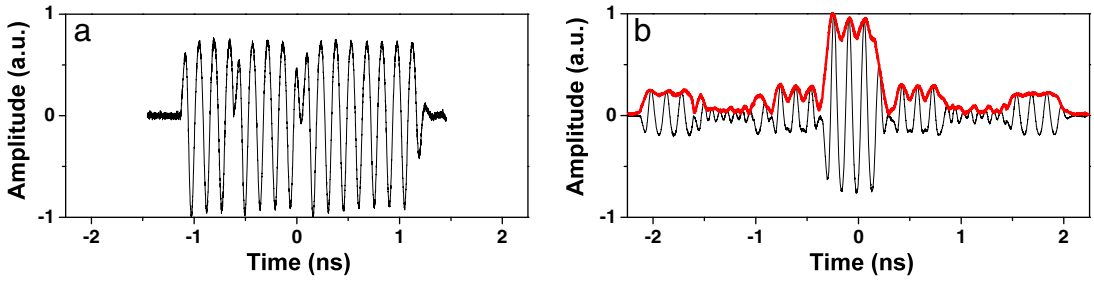

Fig. 18. (a) The input phase-coded microwave signal. (b) The measured correlation output (the black-solid line) with the calculated absolute envelope (the red-solid line).

the tap coefficients, α_k, are optimized to minimize the errors between the desired and the generated chirped pulses. The tap coefficients are calculated to be [1.0, 1.0, 1.0, 1.5, and 1.4]. The dispersive fiber is a length of 25 km standard single mode fiber with a total dispersion of about 425 ps/nm. The generated pulse is then measured by a high-speed oscilloscope, which is shown as the solid line in Fig. 17(a). A chirped microwave pulse having a shape close to the theoretical microwave chirped pulse is generated. A slight distortion in the pulse shape is due to the small tap number. It is known that a chirped microwave pulse can be compressed at a receiver using a microwave matched filter. To demonstrate the pulse compression performance, the correlation between the measured and the reference chirped microwave pulses (the two curves in Fig. 17(a)) is calculated, and the result is shown in Fig. 17(b). It is clearly seen that the microwave pulse is compressed, which confirms that the generated microwave pulse is chirped.

If the input pulse to the delay-line filter has a spectral response that is conjugate to that of the delay-line filter, then the delay-line filter becomes a matched filter, which can be used for pulse compression for applications in radar and microwave imagining systems. The use of the delay-line filter for the compression of a phase-coded microwave pulse was demonstrated [52,55]. Again, the system setup shown in Fig. 16 can be used. The dispersive fiber is a 25-km standard single mode fiber. The output is measured by a high-speed oscilloscope. The input signal has a 6.75 GHz carrier which is phase coded by a 4-chip Barker code, [+1, 1, +1, and +1]. In our design, $m=4$ so that the chip rate is 1.6875 GHz. Then, based on Eq. (54), the time delays for the four taps are calculated which are given [0.5926, 1.1852, 1.8519, and 2.3704] ns. The wavelengths of the four lasers are then calculated according to Eq. (55), which are given [1543.10, 1544.49, 1546.06, 1547.28] nm. The original input phase-coded microwave signal is shown in Fig. 18(a). When the phase-coded signal is sent to the nonuniformly spaced delay-line filter, an auto-correlation is obtained at the output of the filter, which is shown in Fig. 18(b). It is clearly seen that the phase-coded signal is correctly decoded.

6. Discussion and conclusion

Arbitrary microwave waveforms can find many applications such as in radar and communication systems. In most of the applications, microwave arbitrary waveforms are generated using digital electronics, which provides the advantages such as high flexibility and low cost. Due to the limited sampling speed of modern digital electronics, the generation of high-frequency and broadband microwave waveforms is still a challenge. A solution is to use photonics. The high frequency and broad bandwidth offered by modern optics allow the generation of microwave waveforms with high frequency and large bandwidth. In this paper, the techniques to generate arbitrary microwave waveforms based on fiber optics were reviewed. Four different techniques were discussed: direct space-to-time pulse shaping; spectral-shaping and wavelength-to-time mapping; temporal pulse shaping; and microwave pulse generation based on photonic microwave delay-line filters. The advantages of these techniques compared with free-space-optics-based solutions are the simplicity, low cost, and small size. In addition, fiber-optics based systems have high potential for integration. The key limitation of these techniques is the poor reconfigurability. Although some of the techniques could provide limited waveform tunability [18,34], in general, the reconfigurability of the systems is low. For practical applications, a system with large reconfigurability should be employed. The use of integrated optics, such as the silicon-photonic chip-based spectral shaper, as was demonstrated recently [20] and reconfigurable InP-based photonic integrated circuits [56], provides a potential solution for low-cost and large reconfigurable microwave waveform generation.

References

[1] D.E. Leaird, A.M. Weiner, Opt. Lett. 24 (1999) 853.
[2] D.E. Leaird, A.M. Weiner, IEEE J. Quantum Electron. 37 (2001) 494.
[3] D.E. Leaird, A.M. Weiner, Opt. Lett. 25 (2000) 850.
[4] J.D. McKinney, D.E. Leaird, A.M. Weiner, Opt. Lett. 27 (2002) 1345.
[5] J.D. McKinney, D.S. Seo, A.M. Weiner, Electron. Lett 39 (2003) 309.
[6] D.E. Leaird, A.M. Weiner, IEEE J. Quantum Electron. 37 (2001) 494.
[7] J.D. McKinney, D. Seo, D.E. Leaird, A.M. Weiner, J. Lightwave Technol. 21 (2003) 3020.
[8] S. Xiao, J.D. McKinney, A.M. Weiner, IEEE Photonics Technol. Lett. 16 (2004) 1936.
[9] D.E. Leaird, A.M. Weiner, Opt. Lett. 29 (2004) 1551.
[10] D.E. Leaird, A.M. Weiner, S. Shen, A. Sugita, S. Kamei, M. Ishii, K. Okamoto, Opt. Quantum Electron. 13 (2001) 811.
[11] A. Vega, D.E. Leaird, A.M. Weiner, Opt. Lett. 35 (2010) 1554.
[12] Y. Dai, J.P. Yao, J. Lightwave Technol. 26 (2008) 3329.
[13] A.B. Carlson, P.B. Crilly, Communication Systems: an Introduction to Signals and Noise in Electrical Communication, 5th ed., McGraw-Hill, 2010.

[14] M.A. Muriel, J. Azaña, A. Carballar, Opt. Lett. 24 (1999) 1.
[15] J. Chou, Y. Han, B. Jalali, IEEE Photonics Technol. Lett. 15 (2003) 581.
[16] I.S. Lin, J.D. McKinney, A.M. Weiner, IEEE Microwave Wireless Compon. Lett. 15 (2005) 226.
[17] C. Wang, J.P. Yao, IEEE Photonics Technol. Lett. 20 (2008) 882.
[18] C. Wang, J.P. Yao, J. Lightwave Technol. 27 (2009) 3336.
[19] C. Wang, J.P. Yao, IEEE Photonics Technol. Lett. 21 (2009) 793.
[20] M.H. Khan, H. Shen, Y. Xuan, S. Xiao, D.E. Leaird, A.M. Weiner, M. Qi, Nat. Photonics 4 (2010) 117.
[21] C. Wang, J.P. Yao, J. Lightwave Technol. 28 (2010) 1652.
[22] H. Chi, J.P. Yao, J. Lightwave Technol. 26 (2008) 1282.
[23] C. Wang, J.P. Yao, IEEE Trans. Microwave Theory Tech. 56 (2008) 542.
[24] R. Feced, M.N. Zervas, M.A. Muriel, IEEE J. Quantum Electron. 35 (1999) 1105.
[25] O.V. Belai, L.L. Frumin, E.V. Podivilov, D.A. Shapiro, J. Opt. Soc. Am. B 24 (2007) 1451.
[26] J. Skaar, L.G. Wang, T. Erdogan, IEEE J. Quantum Electron. 37 (2001) 165.
[27] E. Peral, J. Capmany, J. Marti, IEEE J. Quantum Electron. 32 (1996) 2078.
[28] H. Xia, J.P. Yao, J. Lightwave Technol. 27 (2009) 5029.
[29] A.M. Weiner, Rev. Sci. Instrum. 71 (2000) 1929.
[30] J.P. Heritage, A.M. Weiner, "Optical systems and methods based upon temporal stretching, modulation and recompression of ultrashort pulses," United States Patent, 1990, No. 4928316.
[31] R.E. Saperstien, N. Alic, D. Pasasenko, R. Rokitski, Y. Fainman, J. Opt. Soc. Am. B 22 (2005) 2427.
[32] J. Azana, N.K. Berger, B. Levit, B. Fischer, Opt. Lett. 30 (2005) 3228.
[33] H. Chi, J.P. Yao, Electron. Lett 43 (2007) 415.
[34] C. Wang, M. Li, J.P. Yao, IEEE Photonics Technol. Lett. 22 (2010) 1285.
[35] M. Li, C. Wang, W. Li, J.P. Yao, IEEE Trans. Microwave Theory Tech. 58 (2010) 2968.
[36] J. Capmany, B. Ortega, D. Pastor, J. Lightwave Technol. 24 (2006) 201.
[37] R.A. Minasian, IEEE Trans. Microwave Theory Tech. 54 (2006) 832.
[38] S. Sales, J. Capmany, J. Marti, D. Pastor, Electron. Lett 31 (1995) 1095.
[39] J. Capmany, D. Pastor, A. Martinez, B. Ortega, S. Sales, Opt. Lett. 28 (2003) 1415.
[40] F. Coppinger, S. Yegnanarayanan, P.D. Trinh, B. Jalali, IEEE Trans. Microwave Theory Tech. 45 (1997) 1473.
[41] J.P. Yao, Q. Wang, IEEE Photonics Technol. Lett. 19 (2007) 644.
[42] F. Zeng, J. Wang, J.P. Yao, Opt. Lett. 30 (2005) 2203.
[43] J.P. Yao, J. Lightwave Technol. 27 (2009) 314.
[44] J.P. Yao, F. Zeng, Q. Wang, IEEE OSA J. Lightwave Technol. 25 (2007) 3219.
[45] Q. Wang, J.P. Yao, Opt. Express 15 (2007) 14667.
[46] M. Bolea, J. Mora, B. Ortega, J. Capmany, Opt. Express 17 (2009) 5023.
[47] H. Mu, J.P. Yao, IEEE Photonics Technol. Lett. 21 (2009) 253.
[48] N. You, R.A. Minasian, IEEE Trans. Microwave Theory Tech. 49 (2001) 2002.
[49] A. Loayssa, J. Capmany, M. Sagues, J. Mora, IEEE Photonics Technol. Lett. 18 (2006) 1744.
[50] Y. Yan, J.P. Yao, IEEE Photonics Technol. Lett. 19 (2007) 1472.
[51] Y. Dai, J.P. Yao, Opt. Express 16 (2008) 4713.
[52] Y. Dai, J.P. Yao, IEEE Trans. Microwave Theory Tech. 58 (2010) 3279.
[53] Y. Dai, J.P. Yao, Opt. Lett. 32 (2007) 3486.
[54] Y. Dai, J.P. Yao, IEEE Photonics Technol. Lett. 21 (2009) 569.
[55] Y. Dai, J.P. Yao, IEEE Photonics Technol. Lett. 21 (2009) 969.
[56] L.A. Coldren, 2010 International Topical Meeting on Microwave Photonics, WE1-1, Montreal, Canada, October 5–9, 2010.